



## Influence of PVDF concentration on the morphology, surface roughness, crystalline structure, and filtration separation properties of semicrystalline phase inversion polymeric membranes

A. Akbari<sup>a,b,\*</sup>, M. Hamadani<sup>a,c</sup>, V. Jabbari<sup>d</sup>, A. Yunessnia Lehi<sup>a</sup>, M. Bojaran<sup>a</sup>

<sup>a</sup>*Institute of Nanoscience and Nanotechnology, University of Kashan, Kashan, Iran*

*Tel. +98 361 4445219; Fax: +98 361 4451495; email: akbari@kashanu.ac.ir*

<sup>b</sup>*Department of Carpet, Faculty of Architecture and Art, University of Kashan, Kashan, Iran*

<sup>c</sup>*Department of Physical Chemistry, Faculty of Chemistry, University of Kashan, Kashan, Iran*

<sup>d</sup>*Anatomical Sciences Research Center, Kashan University of Medical Sciences, Kashan, Iran*

Received 17 July 2011; Accepted 20 February 2012

---

### ABSTRACT

This study was focused on the fabrication of nanoporous poly(vinylidene fluoride) (PVDF) membranes at different polymer concentration (14, 17, and 20 wt%) via phase inversion method. The morphology and surface roughness of the resulting membranes were investigated by scanning electron microscopy (SEM) and atomic force microscope, respectively. SEM results showed that with the increase of polymer concentration, the pore size of membranes and the overall porosity decrease. Also, the results showed that varying concentration results in significant changes on the surface roughness. Analysis of the crystalline structures of PVDF membranes by X-ray diffraction showed that the membranes, which precipitated in the higher concentration of polymer (20 wt%) had a typical “ $\beta$ ” form of the crystalline phase, whereas those membranes that formed at lower concentration (14 wt%) showed crystallites of the “ $\alpha + \beta$ ” form of the crystalline phase. Furthermore, the filtration separation experiments of Acid Yellow 23 (AY23) were conducted to examine the effects of concentration parameter on the performance of nanoporous PVDF membranes. Results showed that the retention of AY23 increases as the polymer concentration increases and an efficiency of 89.72% was achieved in polymer concentration of 20 wt%.

*Keywords:* Poly(vinylidene fluoride); Phase inversion; Membrane; Filtration; Dye Removal

---

### 1. Introduction

As one of the most popular materials for microfiltration (MF) and also ultrafiltration (UF) membranes, poly(vinylidene fluoride) (PVDF) has earned a lot of attention due to its competitive and exceptional properties including impact strength and abrasion resistance, excellent toughness, unsurpassed chlorine

resistance, stability at pH levels from 1 to 11, high ionic purity and low level of insoluble material, excellent UV resistance, low level of extractable material, broad agency approvals (e.g. NSF 61, FDA, USP VI, UL, etc.), readily cast into porous MF and UF flat sheet and hollow fiber membranes, etc. [1,2]. These advantageous properties, coupled with its intrinsic hydrophobic properties, make it an outstanding membrane material particularly for industrial wastewater treatment applications involving oily emulsion [3],

---

\*Corresponding author.

organic/water separations [4], gas absorption and stripping [5], membrane distillation [6], and UF [7].

Thermodynamic characteristics of the initial polymer solution and the as-immersed medium, combined with the kinetic effects of mass transfer of solvent/nonsolvent, determine the ultimate membrane structure in a complex way. A wide variety of experimental parameters have a large impact on the final morphological properties of the membranes, and consequently on their performance [8]. These include the composition of polymer solution (polymer concentration, solvent, cosolvent, additives, and their respective concentrations) [9,10], the type of support material (polymer, glass, metal, nonwovens, etc.) [11], the thickness of the casted polymer film [12], the temperature and time of a possible evaporation step before immersion [13], the temperature and composition of the quenching bath [14], as well as the posttreatment [15] and conditioning of the membrane prior to filtration [16].

In the present study, PVDF membranes with asymmetric structures were prepared by the isothermal immersion precipitation (phase inversion) of PVDF/dimethylformamide (DMF)/H<sub>2</sub>O ternary system in different polymer concentration. The crystalline phase, morphology, surface roughness, and filtration separation capability of resulting membranes were investigated, and the results were discussed and compared.

Despite the large number of publications on the synthesis of polymeric membranes via phase inversion technique, data in studies are seldom linked to a systematic screening of their performance as a membrane. Such an extensive study of the parameters involved in membrane preparation combined with a thorough screening of their performance tends to be time consuming and thus an inefficient route. In this work, in fact, we investigated the physico-chemical properties along with filtration experiments of prepared PVDF membranes. Furthermore, the results of the study were different in comparison with those of other studies [17–24], which are highlighted in the following points: (1) different and various polymer concentrations which were accessible and useful, were

selected and resulted in membranes with nanoporous structures with high porosity and flux values, (2) different morphologies and crystalline structures were observed, and (3) the results showed a high removal of dye (>89%), which shows that such a membrane has a high potential for wastewater treatment.

## 2. Experimental

### 2.1. Materials

Poly(vinylidene fluoride) (PVDF,  $M_w = 534,000$  [GPC],  $d = 1.74 \text{ g/cm}^3$ ,  $m_p = 165^\circ\text{C}$ , Aldrich) and *N,N*-dimethyl formamide (DMF,  $d = 0.94 \text{ g/cm}^3$ ,  $m_p = 163^\circ\text{C}$ , Merck) were used as-received without further purification. Acid Yellow 23 (AY23, Tartrazine) was provided by Alvan Co., Iran. Physico-chemical characteristics of AY23 are presented in Table 1. Deionized water was prepared by an ultrapure water system (Smart-2-Pure, TKA Co., Germany).

### 2.2. Membrane preparation

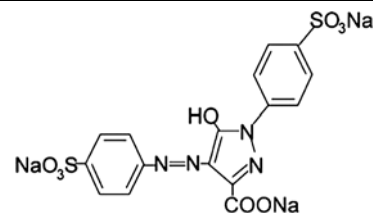
The PVDF was dissolved at  $60^\circ\text{C}$  in the solvent DMF at three different concentrations (14, 17, and 20 wt%, transparent light brown solution). The solution was magnetically stirred for at least one day to guarantee complete dissolution of the polymer. The solutions were cast uniformly onto a glass substrate by means of a hand-casting knife with a knife gap set at  $250 \mu\text{m}$  and then immersed in a coagulation bath at room temperature after exposure for 5 min to air. After complete coagulation, the membranes were transferred into a pure water bath, which was refreshed frequently for at least 24 h to remove the traces of solvent.

### 2.3. Characterizations

Phase analyses of the prepared samples were carried out by powder X-ray diffraction (XRD, Philips X'pert Pro MPD, Holland) using graphite-filtered Cu K $\alpha$

Table 1  
Physico-chemical properties of used dye

Dye	Acid Yellow 23 (AY23)
$\lambda_{\text{max}}$ (nm)	425
Chemical class	Monoazo
C.I.	19,140
$M_w$ (g/mol)	534.37



( $k=0.154\text{ nm}$ ) radiation in the range of  $2\theta$  from  $10^\circ$  to  $40^\circ$ .

The surface morphology of the prepared membranes was observed on a model 1,455 (LEO Co., England) scanning electron microscope (SEM) at an acceleration voltage of 10 kV. Samples for SEM were dried under vacuum, mounted on metal stubs, and sputter-coated with the gold.

Atomic force microscope (AFM) was used to monitor the evolution of surface morphology. AFM allows acquiring 3D topographic data with a high vertical resolution. Accurate and quantitative data about surface morphology are provided over a wide range of magnifications and can be used in several quantitative analyses approaches, such as roughness analysis. AFM measurements were performed using a Nanoscope III scanning probe microscope (Digital Instruments, Santa Barbara, CA, USA) in tapping mode. The membrane sample is mounted on a piezoelectric tube that moves the sample in the  $z$ -direction to maintain a constant force, and in the  $x$ - and  $y$ -directions for scanning the sample. The software directly provides the values for the mean roughness and the number of peaks in the defined area of the membrane.

#### 2.4. Definitions

For the membrane filtration process, the membrane productivity is expressed as the permeate flux through the membrane. The permeate flux is defined as:

$$J_w (\text{l m}^{-2} \text{ h}^{-1}) = \frac{Q}{(A \times t)} \quad (1)$$

where  $Q$  is the volume of permeate (L),  $A$  is the surface area of the membrane ( $\text{m}^2$ ), and  $t$  is the permeate time (h).

The solute rejection ( $R$ ) is defined as:

$$R\% = \frac{C_b - C_p}{C_b} \times 100 \quad (2)$$

where  $C_b$  and  $C_p$  are the concentrations of bulk and permeate solution, respectively.

#### 2.5. Molecular weight cut-off measurements

The main characteristic of a membrane displayed in commercial catalogs is its cut-off (classically noticed molecular weight cut-off [MWCO]). The MWCO is determined by plotting the rejection of solutes such as dextrans and polyethylene glycols (PEGs) against solute MW and interpolating to determine the MW corresponding to a 90% rejection (Fig. 1) [25]. The

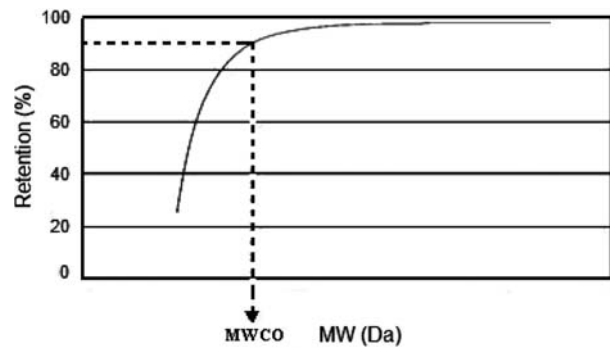


Fig. 1. Schematic diagram of the measurement of membrane MWCO.

sieving effect described that most of the solutes that have larger molecular weight than the MWCO of the membranes, rejected by the membrane, and the ones that have a lower MW than the MWCO of the membrane will permeate easily through the membranes. The average pore diameter of a membrane is difficult to measure directly and must often be inferred from the size of the molecules that permeate or are rejected by the membrane or by some other indirect techniques. The membrane pore size can be estimated by means of solute volume that is rejected by the membrane. Therefore, MWCO can be used for this purpose. The hydrodynamic radius of PEGs can be calculated by using Eq. (6):

$$r_{\text{hyd}} = \left( \frac{3[\eta]MM_{\text{PEG}}}{4\pi\xi N} \right)^{1/3} \quad (3)$$

where

$$[\eta] = 4.9 \times 10^{-8} (MM_{\text{PEG}})^{0.672} \quad (4)$$

$[\eta]$  is the intrinsic viscosity of the solution ( $\text{m}^3 \text{g}^{-1}$ ),  $[\eta]MM_{\text{PEG}}$  is the hydrodynamic volume ( $\text{m}^3 \text{mol}^{-1}$ ),  $\xi$  is the constant proportionality between the radius of the equivalent sphere and the radius of gyration of the polymer molecule (taken as equal to 1), and  $N$  is the Avogadro number ( $\text{mol}^{-1}$ ).

We calculate the MWCO of prepared membranes by plotting PEG with different molecular weight against its retention. The analytical method for determining PEG is given by Sabde et al. [26]. The PEG solutions were analyzed by using spectrophotometry method. PEG solutions were added to the reagents and absorption of the colored mixture was read using a UV–Visible spectrophotometer (GBC, model Cintra 101, Australia) at 535 nm against a blank reagent. Separation experiments using aqueous solutions of the various molecular weights PEG with a concentration

of 2,000 ppm were conducted starting from the lower molecular weight solute. PEGs with different molecular weight purchased from Merck and used as organic additives in dope solution (in membrane preparation) and as a tracer in determining the MWCO.

### 2.6. Dye removal evaluation

The dye removal experiments were carried out with a laboratory-scale filtration unit setup that was designed and manufactured in our laboratory, with an effective surface area of 24 cm<sup>2</sup>. At the beginning of each experiment, the nanofiltration membranes contained in the filtration cells were pressured at 4 bars with deionized water for 2 h to ensure a stable membrane. Then, the feed solution containing predetermined concentrations of dye (70 ppm) was filtered through the filtration system. The operating time required for the filtration system to reach steady state was usually about 30–40 min. The circulating velocity was 8 L/min (a high rectangular flow was used to minimize concentration polarization), pH ~ 7, and the temperature was maintained at 25°C during the experiments. The concentration of the dye was measured by a Shimadzu UV-1700 spectrophotometer. For observed dye removal rate (*R*) by each membrane, at least three trials were carried out and three membrane samples were used per experiment, all the results presented were an average data with standard deviation of the measured values.

## 3. Results and discussions

### 3.1. Morphological study

As the overall composition changes continuously during the phase inversion process, it is clear that the presence of stable or metastable boundaries in addition to the binodal generates a wide range of possible structure formation routes and, consequently, leads to an enhanced variety of potential morphologies. According to previous studies [27,28], the composition of our polymeric solutions (with the exception of 14 wt%) was located in the gelation region. It was in a metastable state with respect to crystallization, and was considered to possess prenucleation embryos that were ready to crystallize upon slight concentration fluctuation. This is attributed to the greater viscoelasticity of a more concentrated polymer solution and entanglements of PVDF chains.

In SEM images of the surface structure of PVDF membranes, many dark spots can be observed (Fig. 2), which may confuse us with the impression that the top surface is porous and not a true skin. In fact, the

dark spots are not pores. They are valleys in the surface topography; this is evident in the AFM images shown in Fig. 3. The valleys could be as small as few tens of nanometers, and some of them are on the scale of a submicrometer [29]. As you see in Fig. 2, when the solution's concentration increases, the number of lowness and highness in membrane surface increases, but their depth decreases [18,20].

For the 14, 17, and 20 wt% casting solution concentrations, noncircular pores were observed in the selective layer. Also, a number of very small pores (<10 nm) can be observed, some of which may interconnect with the macrovoids underneath the skin (Fig. 4). However, in AFM images, we observed an uncommon skin morphology, which differs substantially from that of amorphous membranes. Instead of being continuous and featureless, this top surface comprises nanoscale granular objects of 200–250 nm whose dendritic patterns can also be observed. The boundaries between the granular objects are linear and sometimes rupture into nanocrevice on the surface. The nodules characterizing all PVDF membranes exhibit different size and compactness. In the case of the selective layer, since the concentration increases, membrane skin thickness increases that it influences significantly the inner membrane structure (Fig. 4). Darvishmanesh et al. observed that with increases of casting polymer concentration, the number of pores and macrovoids decreases. Furthermore, they reported that with increases of polymer concentration, the thickness of membrane film increases which resulted in the decrease of membrane flux values [19].

In fact, increasing the concentration causes a decrease in mobility that results in a faster solidification. In the casting solution with high concentration, macromolecules huddle into a dense distribution, i.e. less amount of nonsolvents diffusing into the system results in the demixing of the polymer solution than in a low polymer concentration, which ensures suppressive development of pore in the sublayer. Fig. 4 shows the effect of PVDF concentration on the membrane porous structure. Although no pore former is added into the casting solution, the membrane cast from the dope of 14 wt% shows clear finger-like pores (Fig. 4(A)), and with increase of polymer concentration (20 wt%), finger-like pores are gradually suppressed and slimmed (Fig. 4(C)).

This narrowness and decrease of pore number in membrane can be related to increase of thickness of membrane skin [19]. When the solution concentration increases, amount of polymer in membrane–bath interface increases and results in the decrease of solvent–nonsolvent exchange. A comparison between

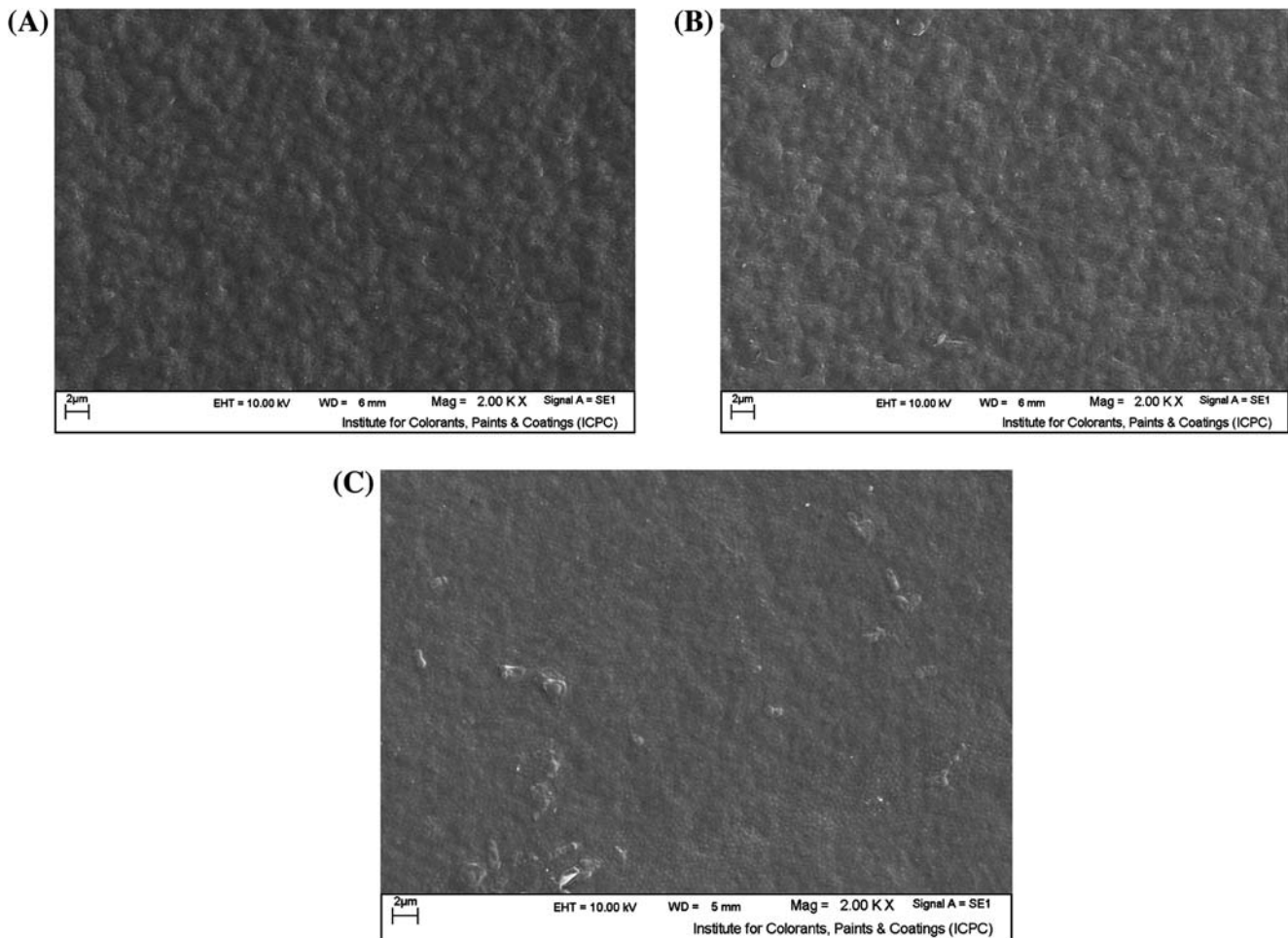


Fig. 2. SEM images of surface structure of nanoporous membranes prepared in different PVDF concentration (A–C: 14, 17, and 20 wt%).

these images indicates that a high polymer concentration indeed results in a less porous membrane with less finger-like pores and macrovoids. As it is obvious from our results (Fig. 4), while the PVDF concentration increases, the thickness of resulting membranes increases which is consistent with the previous results [18,19].

Zhang et al. [20] showed that both the thickness of the top layer and the demixing time increase with the rising polysulfone concentration, mainly because of the hindering effect of viscosity on the diffusion rate between the solvent and nonsolvent. Then, the delayed demixing occurs and thus results in a less porous substructure and a dense, relatively thick top layer. The result is consistent with the research of Reuvers et al. [21,22].

Altinkaya et al. reported the same results. They demonstrated that with increases of cellulose acetate casting solution concentration, the thickness of the

skin layer increased, but the porosity and average pore diameter decreased [30].

In our experiments, the required time for the membranes to detach from the glass substrate was longer at higher concentrations, suggesting correspondingly longer elapsed times. In other words, morphological development appears to be prolonged to a much later stage at higher casting concentration. Specifically, an increase in the concentration of the casting solutions results in the decrease in number and type of chain-like and noncircular pores, which results in a lower flux and higher retention. At a lower concentration, we observed interconnected pore structures in the selective layer of membranes cast (i.e. short solidification times) [19–22].

Furthermore, the number of nuclei of crystallites in solution is increased at a lower concentration in favor of their quicker growth during the formation of the membranes. Indeed, the number of links between the

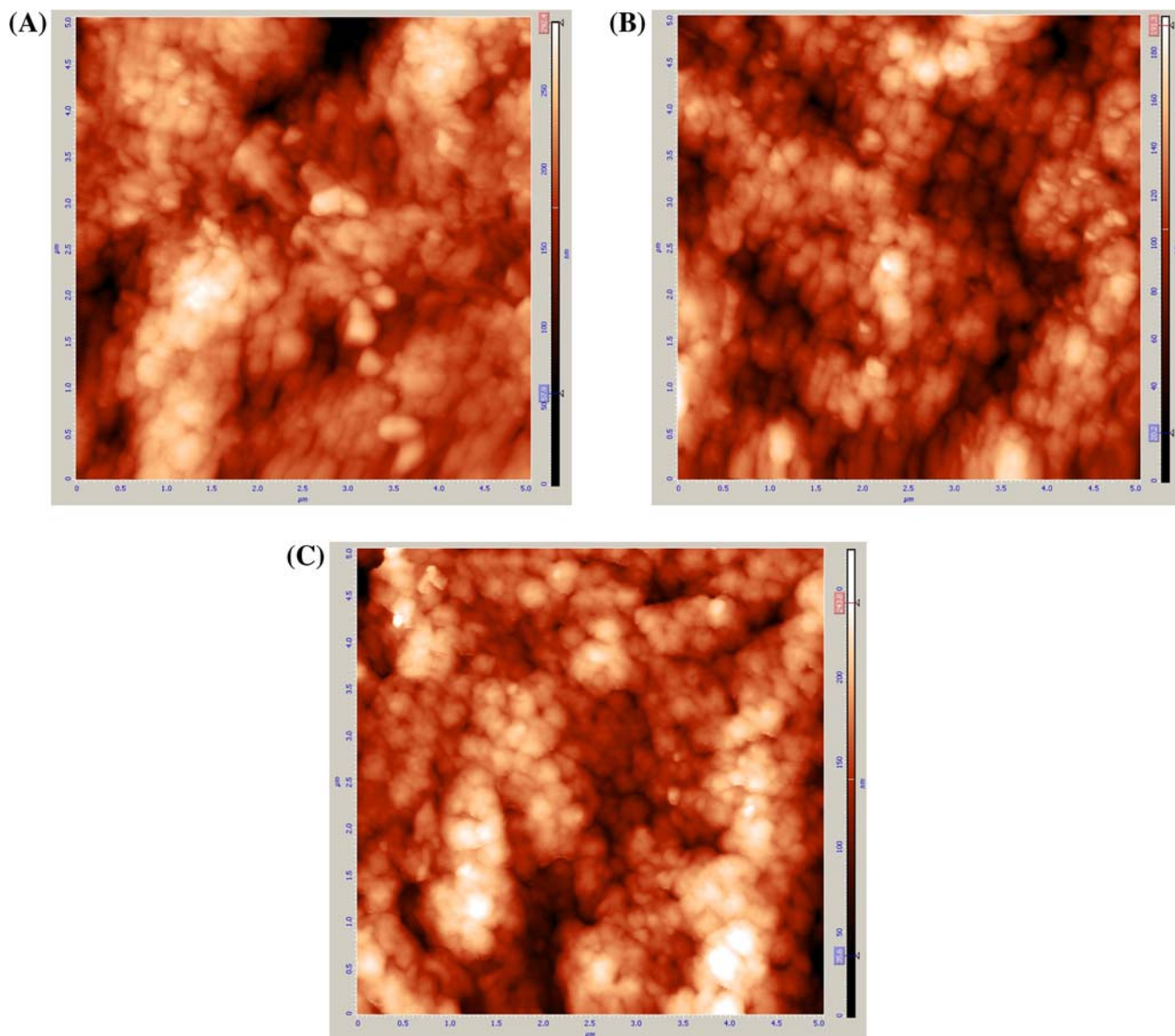


Fig. 3. 2D AFM images of surface structure of nanoporous membranes prepared in different PVDF concentration (A–C: 14, 17, and 20 wt%).

pores is increased, yielding an increase in the void volume fraction. The formation of gaps between the granular objects generates the membrane pores, whose size and distribution are significantly dependent on the membrane's overall porosity (Figs. 3 and 4) [28,31].

In the case of macrovoids, when the concentration increases, approximately the size of macrovoids will be narrowed and shortened [19–21,23]. The walls surrounding the cells are particulate that is indicative of crystallization after the liquid–liquid phase separation (binodal and spinodal decomposition) i.e. when liquid–liquid demixing has completely

established the bulk porous structure, crystallization could only influence the gel phase that surrounds the cellular pores and the rim of macrovoids is packed by arrays of interlinked granular objects (very slow mass exchange). With increasing concentration, their particle size decreases until forming an even surface and the sample becomes less porous and liquid–liquid demixing becomes more dominant. In other words, an interfacial layer with a high polymer concentration was formed around the liquid micelles during phase separation. The micelles grew downward rapidly with the influx of the nonsolvent and solvent to form macrovoids, and the

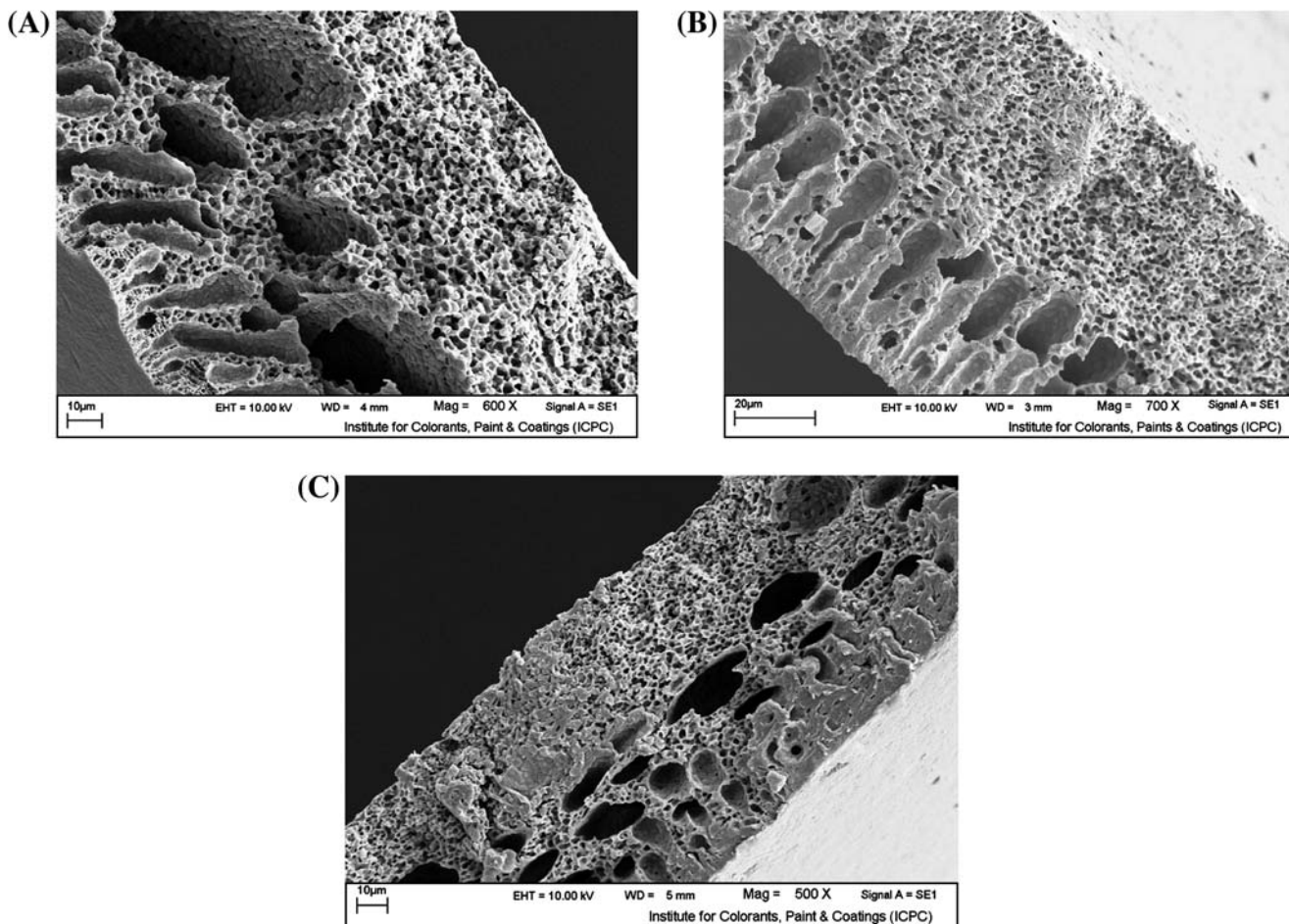


Fig. 4. SEM images of cross-section morphology of PVDF membranes casted in different polymer concentration (A–C: 14, 17, and 20 wt%).

concentrated layer eventually solidified to become a dense wall.

Since the porosity of a membrane depends mainly on the size of these particles, it is expected that the membrane prepared in low polymer concentration has a higher porosity than a higher polymer concentration. In the case of sponge part, as the macrovoids' part will be shortening, approximately it will be larger too. The cellular morphology formed by the growth of liquid micelles against the concentrated phase constituted most of the membrane cross-section [32].

In particular, the images (Figs. 2 and 4) show that increases of polymer content lead to a sharp decline in porosity, which the results agree with those of the study of Mulder [1]. Also, Zhang et al. [20] demonstrated that with the increasing casting polymer concentration, the pore size and porosity of membranes decline sharply from 28.81 to 2.12 nm and 77.41–64.71%, respectively.

### 3.2. Roughness of membranes

Roughness is one of the most important surface properties as it has a strong influence on adhesion (fouling) and also on local mass transfer. Fig. 5 indicates the 3D AFM images of surfaces of PVDF membranes at a scan size of 5 μm. The roughness of membrane surfaces was obtained from the AFM images using SPM software (version 1.4.0.6) for quantitative and qualitative analyses of AFM images. In these images, the brightest area presents the highest point of the membrane surface and the dark regions indicate valleys or membrane pores [33].

Khayet et al. revealed the high effect of polymer concentration on the membrane porosity and roughness. They observed that with increase in PVDF solution concentration, the surface roughness of resulting membrane increases [24]. Also, they observed that permeability decreases and retention increases as the polymer concentration increases. They concluded that

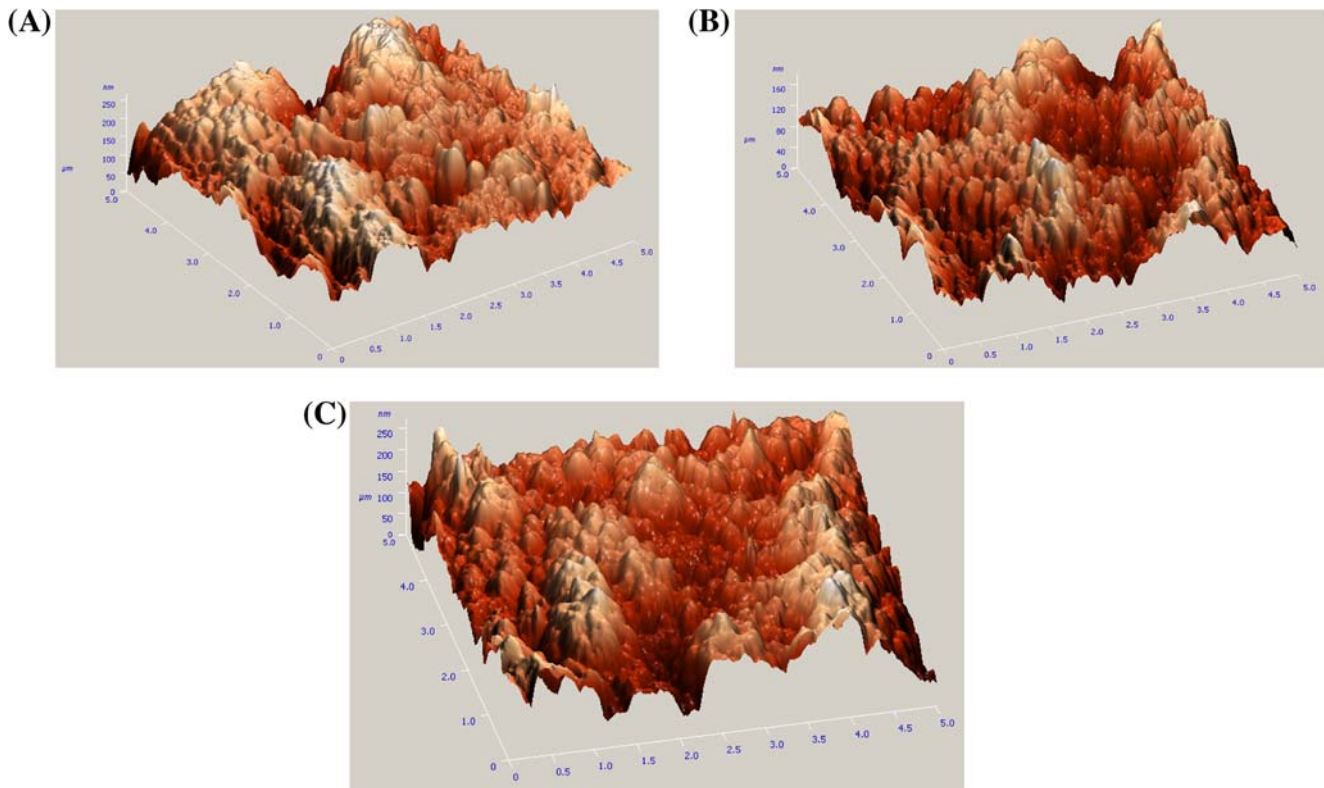


Fig. 5. 3D AFM images of surface structure of PVDF membranes casted in different polymer concentration (A–C: 14, 17, and 20 wt%).

Table 2

Roughness parameters, retention, and flux of the membranes prepared using the phase inversion technique in different PVDF concentration

Polymer concentration (wt%)	Mean roughness ( $R_M$ )	Root mean square roughness ( $R_{RMS}$ )	MWCO (Da)	AY23 retention (%) $\pm 1$	Flux ( $l m^{-2} h^{-1}$ ) $\pm 2$
14	31.3	34.7	18,750	78.64	171
17	30.8	33.8	15,400	83.35	145
20	29.3	32.2	12,700	89.72	180.48

these results are related to the membrane pore size and porosity.

Tiraferri et al. reported that the water flux decreases as the casting polymer content increases from 9 to 18 wt%, which was related to decreases in membrane porosity and number of macrovoids [37,38].

The surface roughness parameters of the membranes are estimated as quantitatively with the following formulas whose results are tabulated in Table 2:

$$R_m = \frac{1}{N} \sum_{i=0}^N |Z_i - Z_{avg}| \quad (5)$$

$$R_{RMS} = \sqrt{\frac{\sum_{i=0}^N (Z_i - Z_{avg})^2}{N}} \quad (6)$$

where  $Z_{avg}$  is the average of  $Z$  in a defined position,  $Z_i$  is the present extent of  $Z$ , and  $N$  is the number of points in the defined position.

This is clear that the morphologies and surface porosities of membranes surfaces strongly change with concentration [34–36]. The roughness parameters for membranes are decreased with an increase in concentration. Generally, the pore size increases as the surface roughness increases and membrane surface exhibits that inherently have distinct peak and valley. The valleys provide paths of least resistance, therefore

a majority of permeate is transported through the membrane via the valley.

In general, as the polymer concentration is raised, the size of granular objects is decreased, which results a decrease in membrane porosity. This is evident from Figs. 3 and 5. So, the concentration is an effective parameter on the membrane roughness.

### 3.3. Identification of membrane crystalline phases

The crystalline phases of PVDF membranes were identified by the XRD patterns. PVDF can be crystallized in four different polymorphs ( $\alpha$ ,  $\beta$ ,  $\gamma$ , and  $\delta$ ) [39,40]. Based on the data reported by Tadokoro et al. [41], we can predict the diffractograms (in the region

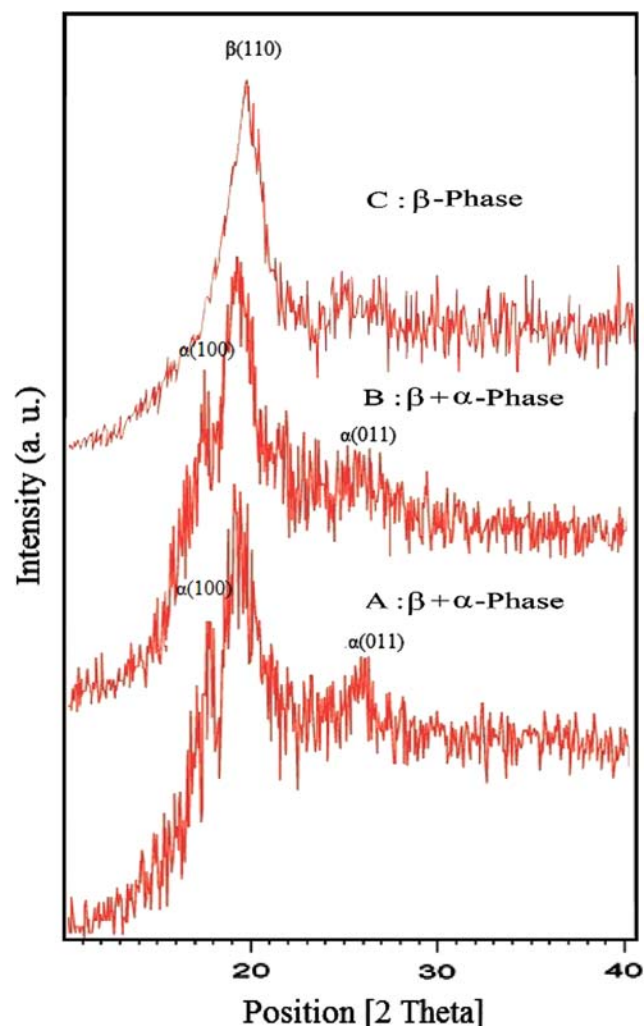


Fig. 6. XRD pattern of PVDF membranes prepared in the different polymer concentration: (A) 14 wt%, (B) 17 wt%, and (C) 20 wt%.

$10 < 2\theta < 50^\circ$ ) which are based on the following parameters:  $\alpha$ -form (monoclinic,  $P2_1/c$  or  $c-C_{2h}^5$ ;  $a=4.96 \text{ \AA}$ ,  $b=9.64 \text{ \AA}$ ,  $c=4.62 \text{ \AA}$ ,  $\beta=90^\circ$ ),  $\beta$ -form (orthorhombic,  $Cm2m$  or  $C_{2v}^{14}$ ;  $a=8.58 \text{ \AA}$ ,  $b=4.91 \text{ \AA}$ ,  $c=2.56 \text{ \AA}$ )  $\gamma$ -phase (monoclinic,  $C121$  or  $C_2^3$ ;  $a=8.66 \text{ \AA}$ ,  $b=4.93 \text{ \AA}$ ,  $c=2.56 \text{ \AA}$ ,  $\beta=97^\circ$ ) [42,43]. The apparent single peak of the  $\beta$ -phase actually comes from the superposition of (200) and (110) reflections. For  $\alpha$ -phase, the peaks are attributed to planes (100), (020), (110), (011), (120), (021), and (111), respectively. The simultaneous presence of  $\alpha$ - and  $\beta$ -phases clearly produces some overlap around  $2\theta=20^\circ$ , which is also more problematic if we consider peak enlargement due to the low crystalline quality of the membranes. The  $\alpha$ -phase can anyway be detected by means of the peaks in the region  $25^\circ$ – $30^\circ$ . All of the membranes shown in Fig. 6 are inherently crystalline, although the morphological characteristics as cellular pores and macrovoids can be ordinarily found in amorphous membranes. The crystalline phase provides thermal stability, while the amorphous phase provides the desired membrane flexibility.

Comparing the crystallographic data of PVDF reported in Fig. 6. Fig. 6(A) and (B) shows that the PVDF crystallites are a mixture of  $\beta$ - and  $\alpha$ -form, the latter being largely in excess. XRD pattern of Fig. 6(A) and (B) represents a typical structure of the PVDF crystallite with the three characteristics multiple peaks at ca.  $19^\circ$ ,  $20^\circ$  and  $27^\circ$ , whose  $\alpha$ -form is only visible in the shoulder at  $2\theta$  of  $19^\circ$  (Fig. 6(A) and (B)). But, for Fig. 6(C), the broad peaks of the  $\beta$  form is clearly dominating the XRD pattern.

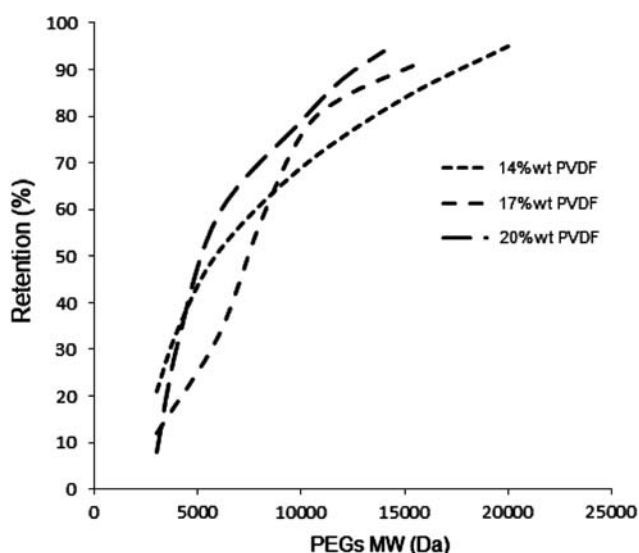


Fig. 7. Determination of MWCO of PVDF membranes prepared at different casting polymer concentration (14, 17, and 20 wt%).

As the results show (Fig. 6), the total crystallinity partially increases as the PVDF concentration increases. The results indicate that the mass exchange rate in viscous casting solutions (e.g. a casting solution with 20 wt% PVDF) is not comparable to that in the lower concentration case, allowing crystallization to commence much earlier to yield higher crystallinity. The  $\beta/\alpha$ -phase ratio decreases with increasing PVDF concentration. This suggests that higher concentration could promote the nucleation of a thermodynamically less stable  $\beta$ -phase. The decrease in the  $\beta/\alpha$ -phase ratio may be ascribed to the significant chain entanglements at high polymer concentration, which lead to the oriented packing of  $\text{CH}_2\text{-CF}_2$  dipoles, thus favoring the formation of  $\beta$ -phase crystals.

### 3.4. Membrane MWCO, pore size, and dye removal measurements

The MWCO results of prepared nanoporous membranes by using 14, 17, and 20 wt% PVDF concentration are presented in Fig. 7. As it is obvious from Fig. 7, the membranes MWCO of 14, 17, and 20 wt% are 18,750, 15,400, and 12,700 Da, respectively. In fact, with increasing concentration of the polymer in solution, the pore size and effective porosity of the membrane decrease (Fig. 8 and Table 2), which result in increases of dye removal and decreases of membrane fluxes [18,19].

Fig. 8 and Table 2 illustrate the retention and flux values of AY23 solution, filtered in 4 bars pressures and 25°C temperature. Table 2 demonstrates that with increases in casted-polymer concentration, the removal of dyes increases, but the flux reduces from 171 to 145  $\text{L m}^{-2} \text{h}^{-1}$  when casted-polymer concentration

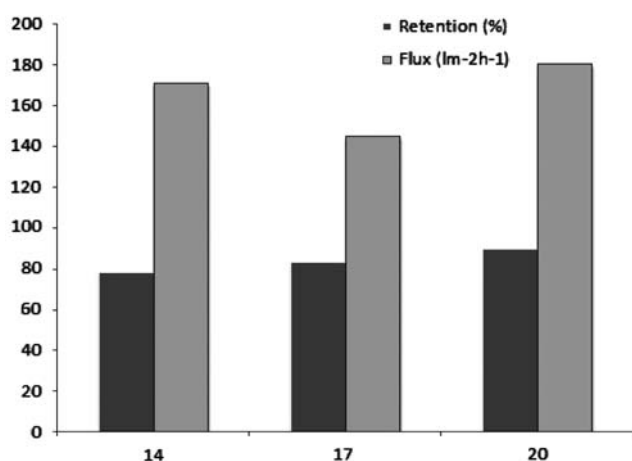


Fig. 8. Retention and flux values of PVDF membranes prepared in different concentration of polymer of 14, 17, and 20 wt%.

increased from 14 to 17%, and then enhances to 180.48  $\text{L m}^{-2} \text{h}^{-1}$  for 20 wt% [19]. The same results were found by previous studies [20–22]. They reported that with increases of polymer concentration, the thickness of the resulting film increases, but porosity, pore diameter, and the number of macrovoids decrease which results in lower fluxes.

## 4. Conclusion

Nanoporous PVDF membranes were successfully fabricated using the wet-phase inversion technique. The physico-chemical characteristics of the resulting membranes have been examined by evaluating the morphology, surface roughness, and crystalline phase. Results showed that the concentration of the casting solution influences the membrane morphology (macrovoids, finger-like). About the crystalline phase, PVDF precipitated into  $\alpha$ -,  $\beta$ -type crystallites at 14 and 17 wt% concentration, but  $\beta$ -type crystallites at 20 wt%. In both cases, the liquid–liquid demixing take place earlier than crystallization considering the unchanged asymmetric finger-like morphology. Furthermore, the removal of more than 89% of AY23 reveals the high potential of prepared PVDF membranes for wastewater treatment.

## Acknowledgments

This study was financially supported by a research grant from the government of Iran. Also, we acknowledge the scholarship, equipment and material support, and study fee waiver provided for A. Akbari by the Institute of Nanoscience & Nanotechnology of University of Kashan.

## References

- [1] M. Mulder, Basic Principles of Membrane Technology, second ed., Kluwer Academic, Dordrecht, 1996.
- [2] J.E. Dohany, L.E. Robb, Polyvinylidene Fluoride Kirk-Othmer Encyclopedia of Chemical Technology, third ed., vol. 11, Wiley, New York, NY, pp. 64–74 1980.
- [3] J.F. Kong, K. Li, Oil removal from oil-in-water emulsions using PVDF membranes, *J. Membr. Sci.* 16 (1999) 83–93.
- [4] K. Jian, P.N. Pintauro, R. Ponangi, Separation of dilute organic/water mixtures with asymmetric poly(vinylidene fluoride) membranes, *J. Membr. Sci.* 117 (1996) 117–133.
- [5] K. Li, J.F. Kong, D. Wang, W.K. Teo, Tailor-made asymmetric PVDF hollow fibers for soluble gas removal, *AIChE J.* 45(6) (1999) 1211–1219.
- [6] M. Khayet, T. Matsuura, Preparation and characterization of polyvinylidene fluoride membranes for membrane distillation, *Ind. Eng. Chem. Res.* 40 (2001) 5710–5718.
- [7] M. Khayet, C.Y. Feng, K.C. Khulbe, T. Matsuura, Study on the effect of a non-solvent additive on the morphology and performance of ultrafiltration hollow fiber membranes, *Desalination* 148 (2002) 321–327.

- [8] R. Ruaan, T. Chang, D. Wang, Selection criteria for solvent and coagulation medium in view of macro-void formation in the wet phase inversion process, *J. Polym. Sci., Part B: Polym. Phys.* 37 (1999) 1495–1502.
- [9] Y.H. See-Toh, F. Castelo Ferreira, A.G. Livingston, The influence of membrane formation parameters on the functional performance of organic solvent nanofiltration membranes, *J. Membr. Sci.* 299 (2007) 236–250.
- [10] N. Leblanc, D. Le Cerf, C. Chappéy, D. Langevin, M. Métaayer, G. Muller, Influence of solvent and non-solvent on polyimide asymmetric membrane formation in relation to gas permeation, *Sep. Purif. Technol.* 277 (2001) 22–23.
- [11] L.E.M. Gevers, S. Aldea, I.F.J. Vankelecom, P.A. Jacobs, Optimization of a lab scale method for the preparation of composite membranes with a filled dense top-layer, *J. Membr. Sci.* 28 (2006) 741–746.
- [12] D.F. Li, T.S. Chung, J.S. Ren, R. Wang, Thickness dependence of macro-void evolution in wet phase inversion asymmetric membranes, *Ind. Eng. Chem. Res.* 43 (2006) 1553–1556.
- [13] N. Leblanc, D. Le Cerf, C. Chappéy, D. Langevin, M. Métaayer, G. Muller, Polyimide asymmetric membranes: Elaboration, morphology, and gas permeation performance, *J. Appl. Polym. Sci.* 89 (2003) 1838–1848.
- [14] S. Fan, Y. Wang, C. Li, K. Lee, D. Liaw, H. Huang, J. Lai, Effect of coagulation medium on membrane formation and vapor permeation performance of novel aromatic polyamide membrane, *J. Membr. Sci.* 204 (2002) 67–79.
- [15] I. Kim, H. Yun, K. Lee, Preparation of asymmetric polyacrylonitrile membrane with small pore size by phase inversion and post-treatment process, *J. Membr. Sci.* 199 (2002) 75–84.
- [16] T. Zhao, Q. Yuan, Effect of membrane pretreatment on performance of solvent resistant nanofiltration membranes in methanol solutions, *J. Membr. Sci.* 280 (2006) 195–201.
- [17] I.M. Wienk, R.M. Boom, M.A.M. Beerlage, A.M.W. Bulte, C. A. Smolders, H. Strathmann, Recent advances in the formation of phase inversion membrane from amorphous or semi-crystalline polymers, *J. Membr. Sci.* 113 (1996) 361–371.
- [18] M.G. Buonomenna, P. Macchi, M. Davoli, E. Drioli, Poly(vinylidene fluoride) membranes by phase inversion: The role the casting and coagulation conditions play in their morphology, crystalline structure and properties, *Eur. Polym. J.* 43 (2007) 1557–1572.
- [19] S. Darvishmanesh, J.C. Jansen, F. Tasselli, E. Tocci, P. Luis, J. Degreve, E. Drioli, B. Van der Bruggen, Novel polyphenylsulfone membrane for potential use in solvent nanofiltration, *J. Membr. Sci.* 379 (2011) 60–68.
- [20] Z. Zhang, Q. An, Y. Ji, J. Qian, C. Gao, Effect of zero shear viscosity of the casting solution on the morphology and permeability of polysulfone membrane prepared via the phase-inversion process, *Desalination* 260 (2010) 43–50.
- [21] A.J. Reuvers, J.W.A. van den Berg, C.A. Smolders, Formation of membranes by means of immersion precipitation. Part I. A model to describe mass transfer during immersion precipitation, *J. Membr. Sci.* 34 (1987) 45–65.
- [22] A.J. Reuvers, *J. Membr. Sci.* 34 (1987) 67–86.
- [23] M. Ramamoorthy, M. Ulbricht, Molecular imprinting of cellulose acetate-sulfonated polysulfone blend membranes for Rhodamine B by phase inversion technique, *J. Membr. Sci.* 217 (2003) 207–214.
- [24] M. Khayet, C. Cojocar, M.C. García-Payo, Experimental design and optimization of asymmetric flat-sheet membranes prepared for direct contact membrane distillation, *J. Membr. Sci.* 351 (2010) 234–245.
- [25] C. Causserand, S. Rouaix, A. Akbari, P. Aimar, Improvement of a method for the characterization of ultrafiltration membranes by measurement of tracers retention, *J. Membr. Sci.* 238 (2004) 177–190.
- [26] A.D. Sabde, M.K. Trivedi, V. Ramachandran, M.S. Hanra, B. M. Misra, Casting and characterization of cellulose acetate butyrate based UF membranes, *Desalination* 114 (1997) 223–232.
- [27] A. Akbari, V. Jabbari, M. Homayonfal, Synthesis and characterization of composite polysulfone membranes for desalination in nanofiltration technique, *Water Sci. Technol.* 62 (2010) 2655–2663.
- [28] J.D. Mendelsohn, C.J. Barrett, V.V. Chan, A.J. Pal, A.M. Mayes, M.F. Rubner, Fabrication of microporous thin films from polyelectrolyte multilayers, *Langmuir* 16 (2000) 5017–5023.
- [29] D.-J. Lin, C.-L. Chang, C.-L. Chang, T.-C. Chen, L.-P. Cheng, Fine structure of poly(vinylidene fluoride) membranes prepared by phase inversion from a water/N-methyl-2-pyrrolidone/poly(vinylidene fluoride) system, *Inc. J. Polym. Sci. Part B: Polym. Phys.* 42 (2004) 830–842.
- [30] S.A. Altinkaya, H. Yenal, B. Ozbas, Membrane formation by dry-cast process model validation through morphological studies, *J. Membr. Sci.* 249 (2005) 163–172.
- [31] M. Wienk, Th. Van Den Boomgaard, C.A. Smolders, The formation of nodular structures in the top layer of ultrafiltration membranes, *J. Appl. Polym. Sci.* 53 (1994) 1011–1023.
- [32] C.A. Smolders, A.J. Reuvers, R.M. Boom, I.M. Wienk, Microstructures in phase inversion membranes. 1. Formation of macro-voids, *J. Membr. Sci.* 73 (1992) 259–275.
- [33] K. Boussu, B. Van der Bruggen, A. Volodin, J. Snauwaert, C. Van Haesendonck, C. Vandecasteele, Roughness and hydrophobicity studies of nanofiltration membranes using different modes of AFM, *J. Colloid Interface Sci.* 286 (2005) 632–638.
- [34] J.Y. Kim, H.K. Lee, S.C. Kim, Surface structure and phase separation mechanism of polysulfone membranes by atomic force microscopy, *J. Membr. Sci.* 163 (1999) 159–166.
- [35] P. Vandezande, L.E.M. Gevers, I.F.J. Vankelecom, Solvent resistant nanofiltration: separating on a molecular level, *Chem. Soc. Rev.* 37 (2008) 365–405.
- [36] A. Bottino, G. Capannelli, A. Comite, Novel porous poly(vinylidene fluoride) membranes for membrane distillation, *Desalination* 183 (2005) 375–382.
- [37] Alberto Tiraferri, Ngai Yin Yip, William A. Phillip, Jessica D. Schiffman, Menachem Elimelech, Relating performance of thin-film composite forward osmosis membranes to support layer formation and structure, *J. Membr. Sci.* 367 (2011) 340–352.
- [38] C.Y. Kuo, H.N. Lin, H.A. Tsai, D.M. Wang, J.Y. Lai, Fabrication of a high hydrophobic PVDF membrane via non-solvent induced phase separation, *Desalination* 233 (2008) 40–47.
- [39] R.J. Gregorio, M.J. Cestari, Synthesis of graft copolymers having phospholipid polar group by micromonomer method and their properties in water, *J. Polym. Sci. Part B: Polym. Phys.* 32 (1994) 859–867.
- [40] C. Barth, M.C. Goncalves, A.T.N. Pires, J. Roeder, B.A. Wolf, Asymmetric polysulfone and polyethersulfone membranes: Effects of thermodynamic conditions during formation on their performance, *J. Membr. Sci.* 169 (2000) 287–299.
- [41] M. Kobayashi, K. Tashiro, H. Tadokoro, Molecular vibrations of three crystal forms of poly(vinylidene fluoride), *Macromolecules* 8(2) (1975) 158–171.
- [42] M. Cakmak, A. Teitge, H.G. Zachmann, J.L. White, On-line small angle and wide-angle X-ray scattering studies on melt-spinning poly(vinylidene fluoride) tape using synchrotron radiation, *J. Polym. Sci. Polym. Phys.* 31 (1993) 371–381.
- [43] P. van de Witte, P.J. Dijkstra, J.W.A. van den Berg, J. Feijen, *J. Membr. Sci.* 117 (1996) 1–31.